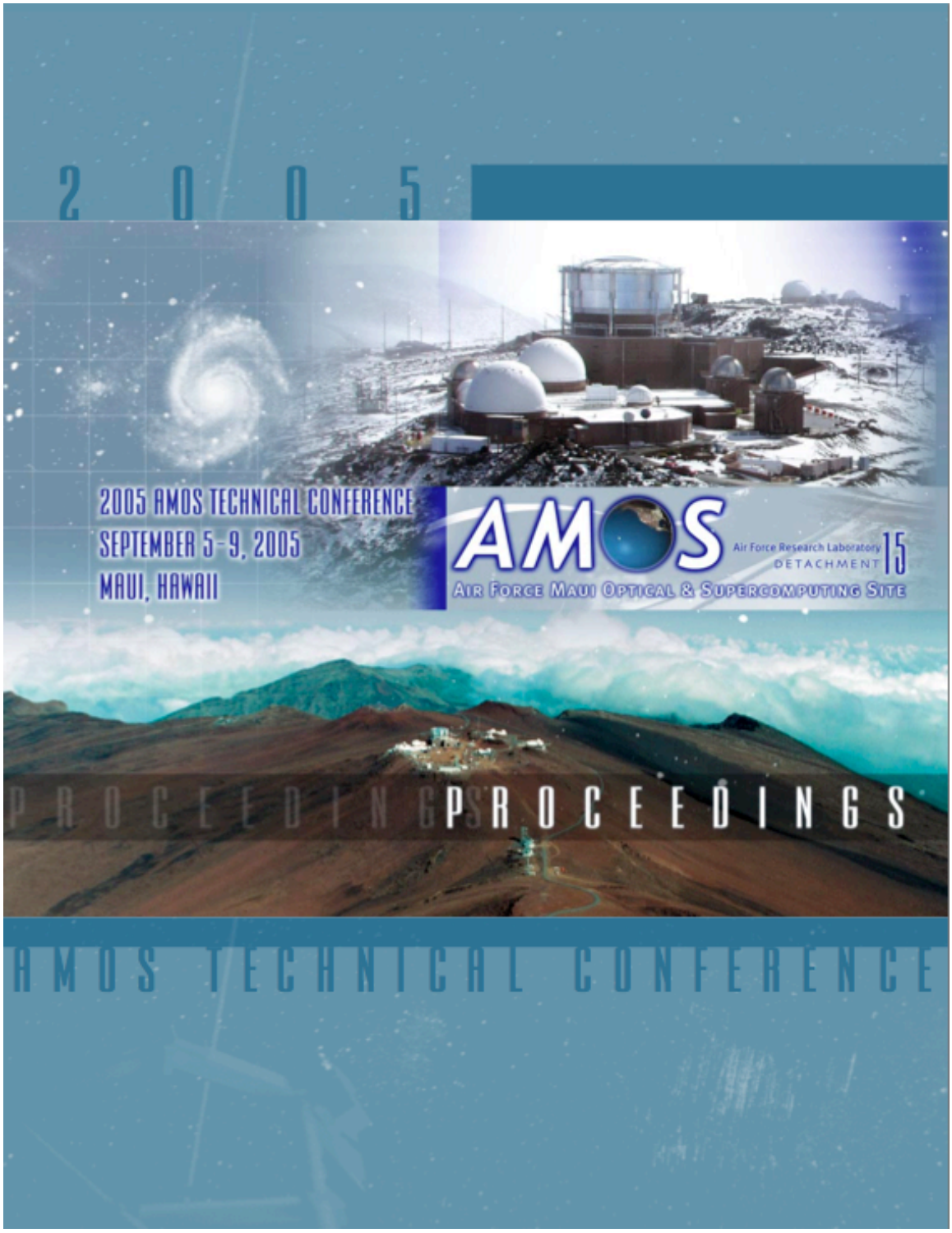

IMAGING (Invited paper)

John McCann, "Rendering High-Dynamic Range Images: Algorithms that Mimic Human Vision", in Proc. AMOS Technical Conference, Maui, p 19-28, 2005.

Rendering High-Dynamic Range Images: Algorithms that Mimic Human Vision

John J. McCann
McCann Imaging, Belmont, MA 02478*

1. ABSTRACT

Receptors in the human retina respond to a range of light that is 10 billion to 1 in radiance. Yet, the optic nerve has a dynamic range of about 100 : 1. In 1953 Kuffler and Barlow showed that the mammalian optic neurons transmitted information about spatial comparisons. Observers easily discriminate details in scenes with dynamic ranges of 10,000 : 1.

High-dynamic-range Retinex algorithms share a common mechanism with vision, namely they are based on spatial comparison of pixels in all regions of the captured image. These algorithms, now available in commercial products, mimic human image processing. They use multi-resolution spatial comparison techniques to render high-dynamic range scenes.

As shown by Ansel Adams, and Jones & Condit, outdoor scenes typically have dynamic ranges of 1000 : 1 in radiances. Scenes with specular reflections, which contain reflected images of the sun, have much greater ranges. Print paper in actual viewing conditions has a dynamic range of less than 100 to 1. Tone-scale transforms, such as S-shaped H&D curves, cannot render output images to match human sensations. Tone-scale transforms compress the highlights and shadows too much. Spatial-comparison algorithms automatically "dodge and burn" the image based on the spatial content of the input image. They automatically generate the equivalent of scene-dependent spatial-frequency filters.

Many other visual phenomena can be modeled by spatial comparisons. Color constancy, visibility of gradients and edges, appearance of transparency, and color gamut transformations are more closely related than one might think. Experiments have shown that they share a common property, namely they can be explained by human spatial-comparison mechanisms.

2. INTRODUCTION

In the second century BC, Hipparchus of Nicea quantized the appearance of stars into six brightness magnitudes. This was the common origin of two scientific measurements. One measures the light coming from celestial bodies and the other measures the response function of the human eye to light. In 138 AD, Claudius Ptolomy described and expanded Hipparcus's stellar magnitude observations in the still extant "Almagest". After many centuries, stellar magnitude is in common use today. It has been modified to be a photometric measurement starting with Pogson in 1856. The stellar magnitude changes by 100 : 1 when the measured luminance changes by 100,000 :1. In other words, stellar magnitudes have a slope of 0.398 (1/2.512) in a plot of log luminance vs. stellar magnitude.[1]

3. MAGNITUDE ESTIMATION OF BRIGHTNESS

Many different authors have measured the change in brightness as a function of luminance. This work is summarized in the Wyszecki and Stiles "Color Science: Concepts and Methods Quantitative Data and Formulae"[2]. Bodmann's magnitude estimation experiments[3] are similar to the conditions in stellar magnitude with a 2° test spot in an 180° surround. Figure 1 replots Bodmann's data. The solid blue line shows the plot of log estimates vs. log luminance. The straight line is similar to Pogson's formula, with a somewhat lower slope (0.3).

In a second experiment, Bodmann changed the surround luminance from 0 to 300 cd/m^2. For spots greater than 300 cd/m^2 the estimates are essentially the same as with no light in the background (dashed blue line). When the test spot is darker than surround, then things become more interesting (red line). The plot of estimates has a much higher slope. Here small changes in luminance generate large changes in appearance. The high-slope behavior, called lightness, has been shown to fit a cube root of luminance function.[4] The cube root has been shown to result from scatter in the intraocular media in the eye. A display of patches made of equal increments in the appearance of lightness will have equal increments of the cube root of luminance. But, after scatter by the intraocular medias, the stimulus on the retinal receptors will be equal increments of log luminance.[5]

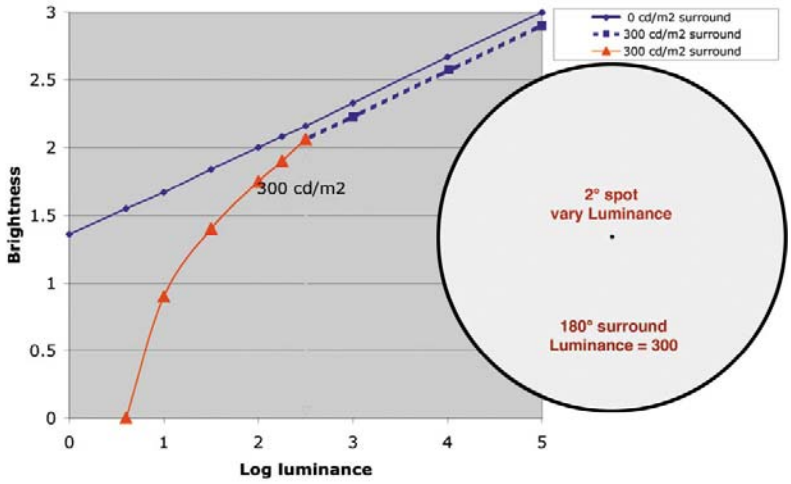

Figure 1 plots estimated brightness vs. log luminance for a 2° test spot viewed on different surrounds. The solid blue line plots observed data for a 0 luminance surround. The dashed blue line shows *spot > surround* data for an 180° surround of 300 cd/m^2. The dotted red line shows *spot < surround* data for the same surround.

The change from low- to high-slope behavior occurs when spot luminance equals surround luminance. Changing the luminance of the surround slides the departure from low-slope behavior to the new matching luminance. We can generalize the data by saying the brightest area in the field of view tracks along a low-slope blue curve in Figure 1. Test spots with lower luminance than the surround exhibit high-slope behavior, regardless of the actual luminance. The mechanism responsible for the appearance of the maxima in the field of view exhibits low-slope dependence on the actual value of luminance. A second, independent, mechanism generates the high-slope behavior from spatial comparisons. It responds to relative, rather than absolute values.

One can use an LCD display as a metaphor for vision. LCD displays have integrated two independent components: one is a uniform light source and the other is a liquid-crystal transmission panels. The light source is the analog of the appearance of the maxima in the field of view. In the LCD the light emitted is controlled by the number of lamps and their power supplies. The light source is the mechanism that controls the maxima in the display image. The liquid crystal panel with polarizers, color filters, transparent electrodes, and pixel signals locally reduce the amount of light to form the rest of image. Analogously, the spatial interactions found in the human visual system control appearance of everything except the maxima. As shown above, these spatial interactions exhibit a high rate of change of appearance with luminance. The maxima exhibit a low rate of change.

3. SPATIAL PROCESSES IN VISION

Over the past century psychophysical and physiological experiments have provide overwhelming evidence that vision is a result of spatial processing of receptor information. Hecht and others showed that threshold detection mechanism use pools of retinal receptors.[6] Rod and cone receptors respond to light over a dynamic range of over 10 billion : 1. That is the range of radiances from snow on a mountaintop to the half-dozen photons needed for a dark-adapted observer to say he saw the light. In 1953 Kuffler[7] and Barlow[8] showed that the signal traveling down the optic nerve has spatial-opponent signal processing. In one example, the center of the cell's field of view is excited by light (more spikes per second). The receptors in the surround of the cell's field of view are inhibited by light (fewer spikes per second). The net result is the cell does not respond to uniform light across its field of view and is highly stimulated by edges. It has the greatest response to a white spot in a black surround. It is important to note that the firing rate of ganglion cells is slightly greater than 100:1. The dynamic range of rod and cone sensors is 10^8 times greater than the dynamic range of the ganglion cells. Dowling[9] showed pre- and post-synaptic behavior of the retina establishing post receptor spatial interactions.

In 1963 Land proposed his Retinex theory[10], asserting that these cone types act as sets, where the response was determined by their spatial interactions. The phenomenon of color constancy is best explained by independent long-,

middle-, and short-wave spatial interactions. Zeki found color constant cells in V4 with predicted spatial properties.[11] Hubel and Wiesel studied the organization of the primary visual cortex's response to stimuli projected on a screen in front of the animal.[12] In each small region of the cortex they found a three-dimensional array of different representations of the visual field. Each segment of the visual field has columns of cortical cells that report on the left-eye image next to a column for the right-eye image. The cells perpendicular to the left/right eye columns respond to bars of different orientations. The third dimension has cells with different retinal size segments of the field of view. Campbell and colleagues showed that there are independent spatial-frequency channels corresponding to bar detectors of different visual angle.[13]

All of this provides a physiological and psychophysical background for making algorithms that mimic human vision. The idea is not to model the actual behavior of visual mechanism, but to abstract its underlying mechanisms. The mechanisms can then be applied to image processing problems.

4. QUANTA CATCH AND APPEARANCE

There are a number of convincing experiments that demonstrate the power and significance of spatial interactions. They share the common theme that identical radiances will generate identical quant catches in the retinal receptors. Identical quanta catches do not generate identical appearances. Identical quanta catches have been shown to produce any color appearance: white, black, red, green, blue, yellow, magenta, cyan, high-chroma and pastel.

Three dramatic experiments are: the Color Mondrian[14], the Black and White Mondrian[14] and real life scenes[15]. The Color Mondrian uses two identical complex arrays of multicolored papers, each illuminated by three (long-, middle-, and short-wave) illuminators. In addition, the experiment used a teleradiometer to measure the light coming to the eye from individual papers in the displays. Measuring a paper in one Mondrian (e.g. dark green) gives readings of L, M, S. Measuring a paper in the other Mondrian (e.g. bright pink) gives readings of L', M', S' in the same illumination. Using the teleradiometer the experimenter increased the long-wave; decreased the middle-wave and increased the short-wave illuminations. These illumination shifts cause the bright pink paper to send L, M, S, identical to the radiances from the dark green paper in the first Mondrian. Observers were asked to describe the color appearances of identical stimuli. They reported that one was dark green, and the other bright pink. They reported that the papers' color appearance was constant. Successively, the experiment tested the full range of colored papers. A single quanta catch generated all color sensations.

The Black and White Mondrian used a single complex array of white, gray and black papers. A single lamp illuminated the display with much more light falling on the bottom than the top. The position of the lamp was adjusted so that the same radiance came to the eye from a white paper on the bottom, as a black paper at the top. Observers reported that the white paper appeared white and the black paper appeared black despite the fact that they had identical radiances, and hence identical quanta catches. [14]

Figure 2 shows a pair of images of a boy holding a white card in the shade. The illumination in the sunlight was 30 times higher than in the shadow. Spot photometer measurements showed that the luminance of the black square in the test target was equal to the white card in the shade. The image on the left shows an S-shaped tone scale photograph taken at the time. All the detail in the sunlight has been lost. The right shows the results of spatial image processing from a digitized image scanned from a long-dynamic-range negative.

The third set of experiments used real life scenes Figure 2 shows a scene with a clear blue sky and a dark shadows under a tree. Spot photometer measurements showed that the light from a white paper in shade was equal to a black paper in sun. Observers reported that the white card looked white, and the black square looked black, regardless of identical luminances. Humans with spatial comparison mechanisms have no difficulty seeing in sun and shade at the same time. S-shaped tone scale photographs cannot render all the details in both sun and shade. [15]

5. DYNAMIC RANGE OF SCENES

In 1939 Ansel Adams first described the zone system for photographic exposure, development and printing.[16] This system extended the photographic sensitometry of Hurter and Driffield[17] and the work of C. K Mees[18,19]. Using a spot photometer Adams would measure the luminance of image segments and assign them to zones in the scale from white to black in the final photographic print. The zone system imposed the discipline of visualizing the final image by assigning image segments to different final print zones prior to exposing the negative. Adams was a trained pianist: He often described the negative as the analog of the musical score and the print as the performance. It was essential that the negative recorded all the information in the scene and that the printing process rendered this information in the print. Photographic contrast, the rate of change of density vs. exposure, is controlled by exposure and development time. Contrast increases with increased development time. Low zone values are controlled by exposure. High values are controlled by development and exposure. The zone system provided the necessary information to select appropriate exposure and processing for each scene's dynamic range. The second stage was to control the amount of exposure for each part of the image (dodge and burn) to render all the desired information from a high dynamic range scene into a low-dynamic range print. Adams described this process in detail for many of his most famous images.[20] He executed remarkable control in being able to reproducibly manipulate his printing exposures so that the final print was a record of his visualization of his image, not a simple record of the radiances from the scene. In fact, Ansel's process was the equivalent of an ***all-chemical*** Photoshop™.

In 1948 Jones and Condit published measurements of the dynamic ranges of 128 real scenes measured by a grease-spot telephotometer.[21] They reported that the minimum range was 1.5 $\log_{10}$ units; the average was 2.2 $\log_{10}$ units; and the maximum was 3.0 $\log_{10}$ units. In 1988 McCann described a technique measuring scene dynamic ranges using a digital scanner.[22] He used slide-duplicating transparency film for recording scenes because of its slope 1.0 response to light. He used a graphic-arts scanner to digitize the film densities. Calibration procedures for the scanner provided images in which digits form 0 to 255 corresponded to log intensities in the scene. As with the Jones and Condit study, a great many scenes were measured with twice the log radiance range as possible to print on paper. Examples were flash exposure, backlit scenes, tungsten and skylight illuminations and sun/shade scenes (Figure 2). All showed ranges of 3.0 $\log_{10}$ units.

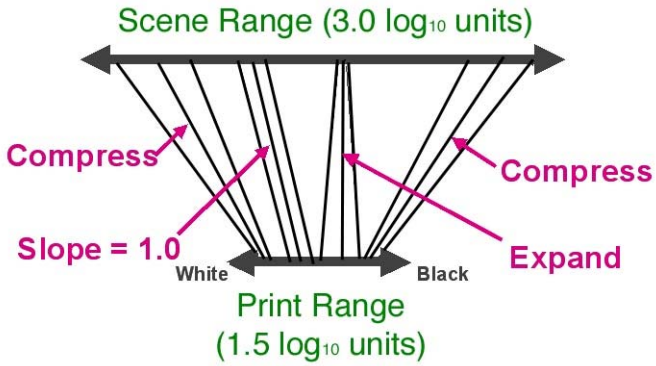

Figure 3 shows the effect of conventional tone-scale mapping. The top line represents 3.0 $\log_{10}$ unit scenes. The bottom arrow represents the 1.5 $\log_{10}$ range of print paper. The s-shaped mapping compresses differences for the highest and lowest radiances. The mid-tones are expanded, giving a color saturation boost to colors such as grass and sky. The slope 1.0 portion of the curve falls in the region of skin tones.

Both chemical and digital photography use a common s-shaped mapping of log radiance to log reflected light from the print. Figure 3 shows the mapping from 3.0 to 1.5 $\log_{10}$ units. Low slope mapping compressed the differences between radiance for the brightest and darkest radiances in the scene. The high-slope portion of the curve expands

the differences between mid-tone radiances. This acts as a color saturation amplifier. The color separation values for blue sky are light gray for the blue record, and medium dark gray for the red and green records. Slopes higher than 1.0 increase the differences between blue and red/green records, thus boosting color saturation. The slope 1.0 portion falls on skin tones and neither compresses nor expands the radiance information.

The most important difference between cameras and human vision is that all cameras count quanta. For any single exposure there is a unique relationship between the quanta caught and the film's or electronic sensor's response. All pixels with the same quanta catch cause the same system response, or reflectance, in the final print. Vision is different, as we saw above (Section 4). Identical quanta catches can generate any color appearance in a single scene. Here, there is no 1:1 mapping as found in single-pixel tone-scale manipulations. A particular quanta catch can generate any response, depending on the rest of the scene. Spatial comparison mechanisms distort the 1:1 mapping and in doing so, compress the large dynamic range found in scenes into much smaller ranges.

6. A SPATIAL MODEL OF VISION

The first spatial model that used the entire scene as input and calculated an output based on spatial comparison was describe in Land and McCann [14] A review[23] of spatial algorithms is found in an Electronic Imaging Symposium, "Retinex at 40"[24]. In principle each pixel in the image can influence every other pixel. Algorithms that compare every pixel with every other pixel carry a very large computational burden. In 1975 Polaroid set up an image-processing lab for the development of imaging algorithms that mimic human vision. Here we developed image segmentation processes so as to involve the entire image but significantly reduce the number of computational steps.[25] At that time, efficient computation of images was essential. If we represent the quanta catch of the scene as an 8-bit log10 image we have two significant advantages. First, 8 bit log is computationally more efficient and convenient than 16-bit linear. Second, vision experiment showed correlation of visual appearance with ratios of radiance. These algorithms use ratios as the first step of spatial comparisons. Ratios of radiance can be very efficiently calculated as the differences of log radiance.

$$\text{RATIO} = [(\log_{10} \text{radiance at x'y'}) - (\log_{10} \text{radiance at x,y})]$$

One efficient algorithm is illustrated in Figure 4. It takes the input (log radiance) image and averages 4 adjacent pixels, thus reducing the size of the image by 4. Repeating this process 8 times generates 384 x256, 192x128, 96x64, 48x32, 24x16, 12x8, 6x4 and 3x2 zoomed input images.

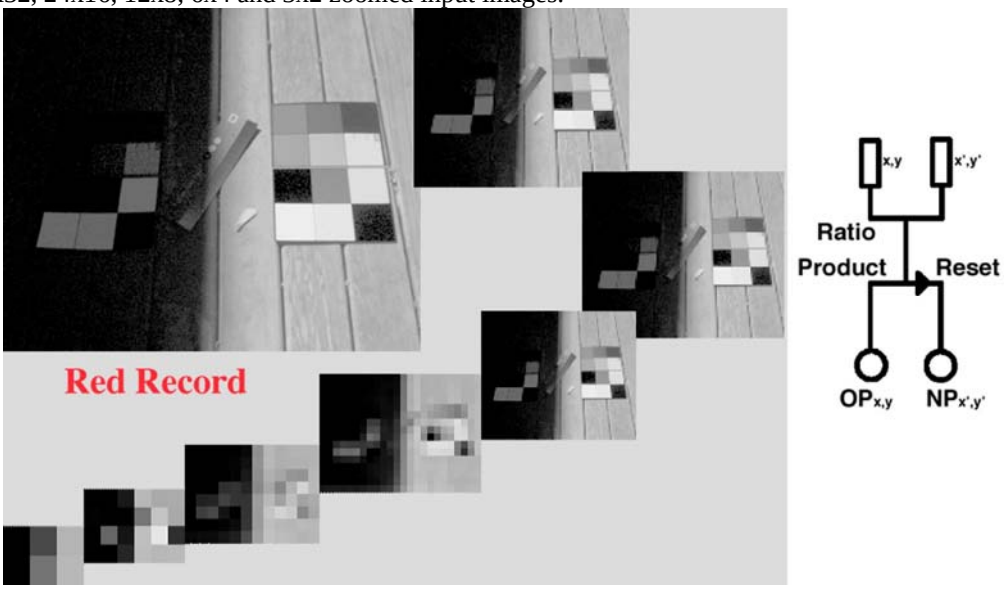

Figure 4 shows the full-resolution red record in the upper left. Each successive image has 1/4 the number of pixels. The bottom left segmentation has only 6 pixels, where the spatial comparisons begin. At each level the ratio, product reset operation is performed and the NEW PRODUCT is extrapolated to be the OLD PRODUCT for the next segmentation.

A spatial comparison process begins by assigning all OLD PRODUCTs to 255, or white. The process calculates the NEW PRODUCT at location x',y' by multiplying the OLD PRODUCT at x,y and the RATIO(x'y'/x,y). It calculates the new estimate of appearance by multiplying the old estimate by the ratio of radiances. Initially, all pixels are assigned the value equal to white. If the ratio is less than 1.0, it reduces the NEW PRODUCT. If the ratio is greater than 1, then the NEW PRODUCT would be greater than 255. However, the RESET step restricts NEW PRODUCT values to a maximum of 255. This is an auto-normalizing step. In the next iteration the NEW PRODUCT is set to be the OLD PRODUCT and the cycle is repeated.

The spatial comparisons begin by calculating the NEW PRODUCTs for 3x2 pixel image. This result is the nearest neighbor interpolated to a 6x4 to be the OLD PRODUCT.[26] The 6x4 input image provides the RATIO data for the NEW PRODUCT calculation. The zoom process is repeated until the NEW PRODUCT output has 384x256 pixels. In this approach all the longest distance interactions are made using only 6 pixels. At each successive iteration, the process becomes more local, until the largest zoom level compares only adjacent input pixels. In a process that compares single pixels at the full resolution with every other pixel, long-distance comparisons are the most computationally costly in time or hardware required. In zoom, multiresolution computations adjacent pixels are the most costly and longest-distance comparisons the most efficient.

The RESET step not only provides auto-normalization, but also makes the process sensitive to the number of iterations. With a few iterations the output is highly influenced by the initial condition that all pixels are equal to white. With very high numbers of iterations the output values approach the input values. Here again we can look to vision appearance experiments for tuning the model. The well-known Simultaneous Contrast experiment (Figure 5) has two identical gray squares on different white and black backgrounds.

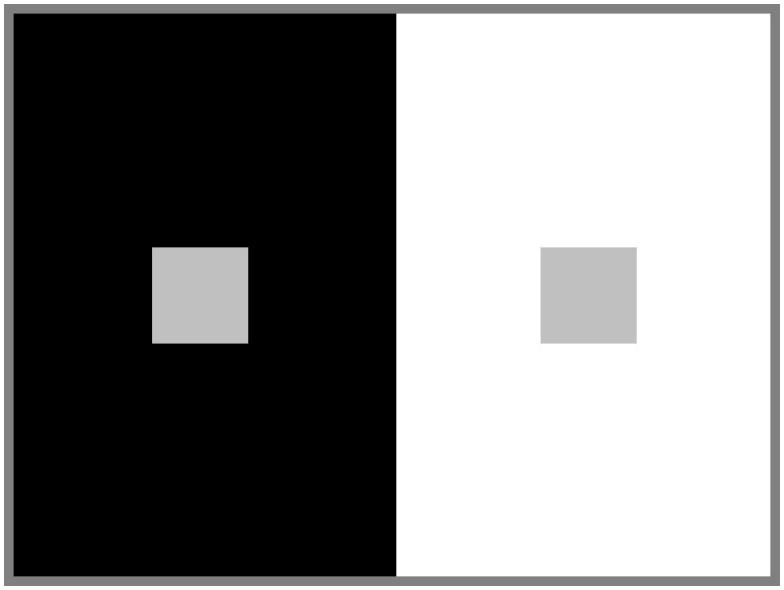

Figure 5 shows Simultaneous Contrast. If spatial interactions were global, then the appearance of two identical gray squares should look the same. The gray in black looks lighter than the gray in white. Yet it does not look white, as expected by a purely local process. Spatial interactions are neither global, nor local.

If vision had perfect long-distance interactions then these two gray patches should appear identical. Their reflectances are the same, so any iterative process that went to completion would result in the prediction of equal gray appearances. By contrast, any purely local auto-normalizing process would make the gray in black be equal to white. That gray is the maximum in the entire neighborhood and would be transformed to be equal to white. Visual processing does neither of these extremes. It is neither global, nor local, but somewhere in between. This simultaneous contrast target is sensitive target for tuning algorithms.[27] The gray in black is 10% lighter than the gray in white. Searching for the best results for this image will produce an algorithm that works for most images.

One can use low-spatial frequency filters to model simultaneous contrast. By picking the right spatial frequency and amplitude one can make the gray on black 10% lighter.[28] This just postpones the problem because vision applies different spatial-frequency filter to different scenes. This can be seen by matching appearances of gray patches in each of white, gray and black surrounds. A selection of grays are darkest in a white surround. This is the equivalent of no low-spatial-frequency filter. The same grays in a gray surround appear lighter. This is the equivalent of a strong low-spatial-frequency filter. The same grays in a black surround appear much lighter. This is the equivalent of a very strong low-spatial-frequency filter. The RESET mechanism, with an intermediate number of iterations, has the unusual property of producing different outputs depending on the properties of the image. Although a low-spatial-frequency filter can accomplish the same thing, they require an additional logical step in analyzing the image so as to determine the frequency and amplitude of the filter for each scene.

Figure 6 illustrates the process of a spatial algorithm. The input sun/shade image (upper left) has a white square in the shade with the nearly same digital values as a black square in the sun. (See top right -"Masked Input" -A gray mask covers the image adjacent to the squares in question.) The algorithm described in Figure 4 processes the RGB separations separately.[29] Iterations of spatial comparisons auto-normalizes the separations and significantly reduces their range of digits. These range-compressed images are now scaled by a post-lut to restore the image to the full 0-255 range and to shape the tone scale of the processed image to fit the output device such as a display or printer.[30] The output separations are in the lower center. The digital values of the white and black squares are no longer equal (See bottom right -"Masked Output"). The digital value of the white in the shade is now much greater than the black in the sun. The recombined RGB separations are shown in the full color image on the bottom left. The output image shows much more detain in the shadow, while having very little adverse effect on the sun part of the image.

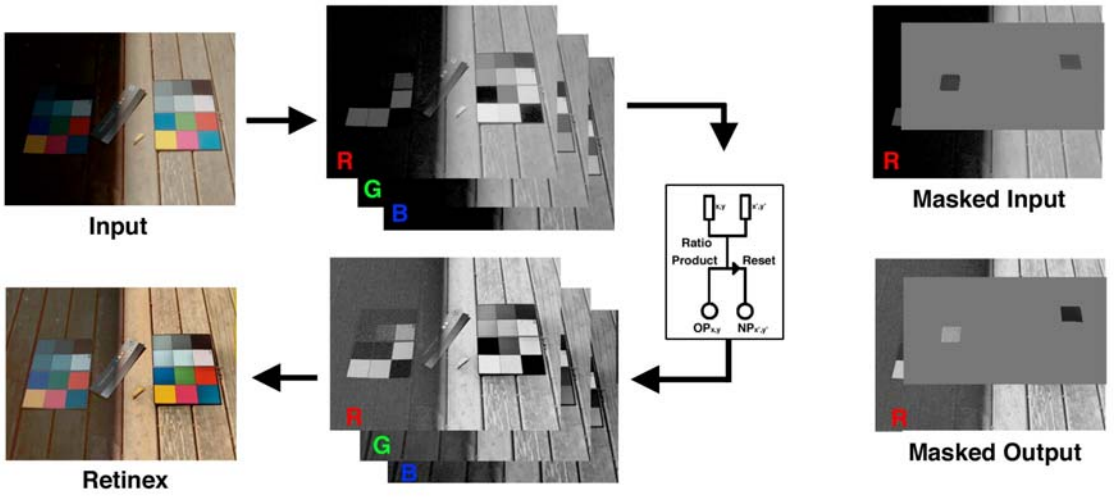

Figure 6 shows the processing steps in a multiresolution spatial comparison algorithm. The color input is on the top left. Its three separations are processed independently (Figure 4). The top-right image shows a gray mask placed over the R separation, but leaving the white/shade and black/sun areas uncovered. They are equal. Spatial processing calculates new separations (bottom center). The mask over the output R separation shows that the white/shade is much lighter than the black/sun area. The color output image is seen on the bottom left.

8. EXAMPLES OF PROCESSED IMAGES

There are a number of related spatial operators.[31] A special edition of the Journal of Electronic Imaging published the papers in the "Retinex at 40" symposium.[24] Figure 6 is an image processed in the manner described above. Below that (Figure 7) is an image processed by Bob Sobol of HP[32]. The final image (Figure 8) shows a comparison is a Kauain chicken photographed with an HP 945 camera using "Digital Flash", a feature using a Sobol version of Retinex processing. In all cases the left image is the control image showing the conventional image; the right image shows spatial-dynamic-range compression based on Retinex.

Figure 7 shows the conventional digital image on the left and that same image processed in the manner described above.

Figure 8 (left) shows a conventional digital image taken by Ken Hall; (right) shows that same image processed by Bob Sobol's algorithm.

Figure 9 (left) shows a conventional digital image taken with a HP 945; (right) shows a second picture using Retinex based "Digital Flash".

DISCUSSION

Many other visual phenomena can be explained by the influence of spatial comparisons. Color constancy can be successfully modeled by independent auto-normalization of sets of cones.[33] Further, the departures from perfect constancy can be understood by the spectral crosstalk of cone-sensitivity functions.[34,35] The visibility of gradients is different from the visibility of edges. This can be understood as the result of highly nonlinear processes such as reset. The appearance of transparency correlates with constant edge ratios.[36] Color gamut transformations, such as display to printer, can produce improved images by maintaining spatial relationships rather than using colorimetric matches.[37]. In this case images with the highest colorimetric error are the best reproductions. All these experiments share a common property with dynamic range compression, namely they can be explained by human spatial-comparison mechanisms.

9. SUMMARY

Stellar magnitude is an excellent example of how human vision responds to maxima in scenes. It exhibits a low-slope response changes in quanta catch by retinal receptors. What makes the study of human vision very interesting is that the physiology of the retina and cortex use spatial interaction to produce a second type, high-slope, of responses to light. Innumerable experiments show the highly nonlinear characteristics of spatial comparisons. They are more than local interactions, but less than global. Multi-resolution algorithms that propagate local comparisons across the entire image work well in dynamic-range compression, just as long as the process has nonlinearities consistent with human vision. Examples here show the advantages of high-dynamic compression algorithms making objects in shadows more visible.

10. ACKNOWLEDEMENTS

The author wants to thank Keith Knox for the invitation to participate in the AMOS conference, and Alesandro Rizzi for discussions that led to this review.

11. REFERNCES

* mccanns@tiac.net

[1] R. E. Zissell, *Evolution of the "Real" Visual Magnitude System*, JAAVSO **26**, 151, 1998.
[2] G. Wyszecki and W. S. Stiles, *Color Science: Concepts and Methods Quantitative Data and Formulae*, 2nd Ed, John Wiley & Sons, New York, 486-513, 1982.
[3] H. W. Bodmann, P. Haubner and A. M. Marsden, *A Unified Relationship between Brightness and Luminance*, CIE Proc. 19th Session (Kyoto) 99-102, 1979, CIE 50-1979.
[4] CIE, *Recommendations on Uniform Color Spaces Color Difference Equations Psychometric Color Terms*, Supplement No. 2 of CIE Publ. No 15 (E-1.3.1) 1971 Bureau Central de la CIE Paris 1978.
[5] W. A. Stiehl, J. J. McCann and R. L. Savoy, *Influence of Intraocular Scattered Light on Lightness-Scaling Experiments*, J. Opt. Soc. Am. **73**, 1143-1148, 1983.
[6] H. Davson, *The Eye: The Visual Process Vol 3*, Academic Press, New York, 1962.
[7] S. W. Kuffler, *Discharge Patterns and Functional Organization of the Mammalian Retina*, J. Neurophysiol.,**16**, 37-68, 1953.
[8] H. B. Barlow, *Summation and Inhibition in the Frog's Retina*, J. Physiol., **119**, 69-88, 1953.
[9] J. E. John E. Dowling, *The Retina: An Approachable Part of the Brain*, Belknap Press, 1987.
[10] E. H. Land, *The Retinex*, Am. Scientist, **52,** 247-264, 1964.
[11] S. Zeki, *Vision of the Brain*, Blackwell Science Inc., Williston, Vermont, 1993.
[12] D. H. Hubel and T. N. Wiesel, *Brain and Visual Perception*, Oxford University Press, 2005.
[13] C. Blakemore C. and F. W. Campbell, *On the existence of neurons in the human visual system selectively sensitive to the orientation and size of retinal images*, J. Physiol., Lond. 203, 237-260, 1969.
[14] E. H. Land and J. J. McCann *Lightness and Retinex Theory*, *J. Opt. Soc. Am.* **61** 1-11, 1971.
[15] J.J. McCann, *Lessons Learned from Mondrians Applied to Real Images and Color Gamuts*, Proc. IS&T/SID Seventh Color Imaging Conference, 1-8, 1999.
[16] A. Adams, *The Negative*, New York Graphical Society, Little, Brown & Company, Boston, 47-97, 1981.
[17] F. Hurter and V. C. Driffield, "*The Photographic Ressearches of Ferdinand Hurter & Vero C. Driffield*", W. B. Ferguson, Ed., Morgan and Morgan Inc. Dobbs Ferry, 1974.
[18] C. E. K. Mees, *An Address to the Senior Staff of the Kodak Research Laboratories*, Kodak Research Laboratory, Rochester, 1956.
[19] C. E. K. Mees, *Photography*, The MacMillan Company, 1937.
[20] A. Adams, *Examples: The Making of 40 Photographs*, New York Graphical Society, Little, Brown and Company, Boston, 1984.
[21] L. A. Jones and H. R. Condit, *J. Opt. Soc. Am.* **38,** 1-11, 1948.
[22] J. J. McCann, *Calculated Color Sensations applied to Color Image Reproduction*, in Image Processing 3Analysis Measurement and Quality, Proc. SPIE, Bellingham WA, **901**, 205-214, 1988.
[23] J. J. McCann, *Black Capturing a black cat in shade: past and present of Retinex color appearance models*, Journal of Electronic Imaging, **13**, 36-47, 2004.
[24] J.J. McCann, ed., *Retinex at Forty*, Journal of Electronic Imaging, **13**, 1-145, 2004.
[25] J. Frankle and J. J. McCann *Method and apparatus of lightness imaging, U. S Patent* 4384336, May 17, 1983.
[26] W. R. Wray, *Method and Apparatus for Image Processing with Fields Portions*, U.S. Patent, 4,750, 211, June 7, 1988.
[27] J. J. McCann, *Simultaneous Contrast and Color Constancy: Signatures of Human Image Processing* in Proc of 9th. Annual Vancouver Cognitive Science Conference Colour Perception: Philosophical Psychological Artistic and Computational Aspects Oxford Press, 88-101, 2000.
[28] T. P. Stockham, *Image Processing in the Context of a Visual Model*, Proc. IEEE, 60, 828-284, 1972.
[29] Other variations convert RGB to YCC, process the Y separation, and convert back to RGB. This process works very well. The separate RGB process provides a mechanism for automatic color balance of the image, but has greater processing time, if color balance is not required.
[30] B. V. Funt, F. Ciurea, J. J. McCann, *Retinex in MATLAB™*, J. Electronic Imaging, **13**, 48-57, 2004.
[31] A. Rizzi, C. Gatta, D. Marini, *A New Algorithm for Unsupervised Global and Local Color Correction, Pattern Recognition Letters*, **24**, 1663-1677, 2003.
[32] R. Sobol, *Improving the Retinex algorithm for rendering wide dynamic range photographs*, Journal of Electronic Imaging, **13**, 65-74, 2004.
[33]J. J. McCann S. McKee & T. Taylor, *Quantitative studies in Retinex theory: A comparison between theoretical predictions and observer responses to 'Color Mondrian' experiments*, Vision Res. **16** 445-458, 1976.
[34] J. J. McCann, *Mechanism of Color Constancy*, 12th IS&T/SID Color Imaging Conference, Scottsdale, **12**, 29-36, 2004.
[35] J. J. McCann, *Do humans discount the illuminant?*, in Human Vision and Electronic Imaging X, B. E. Rogowitz, T. N. Pappas, S. J. Daly, eds. SPIE, Proc. Electronic Imaging, **5666**, 9-16, 2005.
[36] C. Ripamonti, S. Westland, O. da Pos, *Conditions for perceptual transparency*, J. Electronic Imaging, **13**, 29-35, 2004.
[37] J. J. McCann, *A Spatial Gamut Mapping Calculation to Optimize Colour Appearance*, in *Colour Image Science: Exploiting Digital Media*, L. MacDonald and M. R. Luo , Eds., 213-233, 2002.